Angular-dependent asymmetries of above-threshold ionization in a two-color laser field

Siqiang Luo,[1] Min Li,[1,*] Hui Xie,[1] Peng Zhang,[1] Shengliang Xu,[1] Yang Li,[1]
Yueming Zhou,[1] Pengfei Lan,[1] and Peixiang Lu[1,2,†]

[1]*School of Physics and Wuhan National Laboratory for Optoelectronics, Huazhong University of Science and Technology, Wuhan 430074, People's Republic of China*

[2]*Laboratory of Optical Information Technology, Wuhan Institute of Technology, Wuhan 430073, People's Republic of China*

(Received 2 May 2017; revised manuscript received 12 July 2017; published 21 August 2017)

We measure photoelectron momentum spectra from above-threshold ionization of Xe atoms in a linearly polarized two-color laser field with comparable intensities. The spectra show distinct forward-backward asymmetries along the laser polarization direction, which depend sensitively on the electron emission angle and the relative phase between the two-color components. We find that with increasing the emission angle relative to the laser polarization direction, there is a phase shift in the asymmetry curve as a function of the two-color relative phase. Using a semiclassical model, we disentangle the relative contributions of the nonscattering and the rescattering trajectories on the photoelectron angular distributions of the above-threshold ionization. We show that the angular-dependent asymmetry comes from different contributions of the nonscattering and rescattering trajectories at different emission angles. By tuning the relative phase of the parallel two-color laser fields, the relative contributions of the nonscattering and the rescattering trajectories can be precisely controlled.

DOI: 10.1103/PhysRevA.96.023417

I. INTRODUCTION

Above-threshold ionization (ATI) is one of the most fundamental processes in strong-field physics, which has attracted both experimental and theoretical interest in the past three decades [1]. ATI is interpreted as multiphoton absorption beyond the threshold when the Keldysh parameter [2] γ is larger than 1 ($\gamma = \sqrt{I_p/2U_p}$ where I_p is the ionization potential, $U_p = {F_0}^2/4\omega^2$ the ponderomotive energy, F_0 the field amplitude, ω the laser frequency). Atomic units (a.u.) are used throughout unless stated otherwise. In the tunneling regime, i.e., $\gamma < 1$, a series of electronic wave packets are released at the tunnel exit, which follow different pathways from a specific electronic initial state into the same final momentum. The formation of the photoelectron angular distributions of the ATI has been revealed in terms of the interference of the trajectories [3,4].

In the ATI energy spectra, it is believed that the electrons with energy smaller than $2U_p$ are mainly dominated by nonscattering trajectories. Besides those nonscattering trajectories, rescattering trajectories also make a considerable contribution to the ATI energy spectra. It is well known that electron rescattering plays an important role in the formation of high-order ATI; i.e., the rescattering electrons can form a plateau in the ATI energy spectrum ranging from $\sim 2U_p$ to a cutoff at $10U_p$ [5]. Recently, it has been shown that the rescattering trajectory has a significant effect on the spider-leg-shaped structures in the momentum distribution of the low-energy electrons [6,7]. Both rescattering and nonscattering trajectories have been successfully used to image molecular orbitals [8–10]. In addition, the rescattering trajectories are also very significant for the related strong-field processes, such as nonsequential double ionization [11], high-order-harmonic generation [12,13], and molecular dissociation and fragmentation.

The above-threshold ionization by two-color laser fields with well-defined relative phase allows one to control tunneling electrons with attosecond precision [14]. It has been shown that the photoelectron energy spectra and the doubly differential momentum distributions of the ionized electron vary sensitively with the relative phase in a two-color laser pulse consisting of the fundamental field and its second harmonic [15–17]. Those strong variations have many applications in strong-field physics. Using a two-color laser pulse, one can control the photoelectron interferences in both temporal and spatial domains [18–21], the electron-electron correlation in nonsequential double ionization [22], and the proton emission in molecular dissociation [23]. Nowadays, the two-color laser fields have further extended to probing phase shifts and electron delays in ATI [24], retrieving the phase difference of the valence-electron cloud in atoms [25], determining the ionization and tunneling times of high-harmonic generation [26,27], and measuring the Freeman resonance delay between electrons emitted via two Rydberg states [28]. Using the phase-of-the-phase spectra, Skruszewicz *et al.* have revealed the subcycle dynamics of the high-energy rescattering electron in a parallel two-color field [29]. Most of the previous experimental works investigated the energy-resolved electron spectra with respect to the relative phase in a two-color laser field [24,28]. The angle-dependent electron spectrum of the ATI with respect to the relative phase is rarely studied.

In this work, we measure the photoelectron momentum spectra from above-threshold ionization of Xe atoms in a two-color laser field with parallel polarizations using velocity-map imaging (VMI) spectrometers. The angle-resolved electron spectra of the ATI show distinct oscillations with respect to the relative phase of the two-color components. Depending on the electron emission angle, the electron yield shows obvious forward-backward asymmetries along the laser polarization direction. We find that with increasing the emission angle relative to the polarization direction, there is a phase shift

*mli@hust.edu.cn
†lupeixiang@mail.hust.edu.cn

in the asymmetry curve with respect to the two-color relative phase. Based on a semiclassical model, we separate the relative contributions of nonscattering and rescattering trajectories on the photoelectron angular distribution of the ATI. The relative contributions of the nonscattering and the rescattering trajectories to different emission angles differ considerably, thus leading to the angular-dependent asymmetries. The nonscattering electrons are mainly distributed in the laser polarization direction, while the rescattering electrons can be emitted to the direction with a large angle relative to the laser polarization depending on the relative phase of the two-color components. Through tuning the relative phase, the relative contributions of the nonscattering and the rescattering trajectories can be precisely controlled in the parallel two-color laser field.

II. METHODS

A. Experiment

The experiments were carried out using a homebuilt VMI spectrometer [30]. The laser pulse generated by a Ti:sapphire laser system (800 nm, 35 fs, 1 kHz) was used to produce the second harmonic with a 300-μm-thick β-barium borate (β-BBO) crystal. After the BBO, the laser pulse consisted of both fundamental (800-nm) and second-harmonic (400-nm) components, and they were sent through a calcite plate to compensate the group delay between the two colors introduced by the rest of the optical elements. Then we sent the pulse through a dual-order wave plate to rotate the polarization of the 800-nm component while keeping the polarization of the 400-nm field unchanged. The two-color field was passed through a wire grid polarizer to ensure that the two-color components had the same polarization direction. The polarization direction of the laser beam was parallel to the MCP detector and perpendicular to the static electric field of the VMI. We changed the relative phase between the two-color components with a pair of glass wedges. One of the wedges was fixed, and the other one was mounted on a motorized stage. The two-color laser pulse was focused into the VMI spectrometer to interact with the gas beam of Xe using a convex lens. To have a high resolution of the low-order ATI, we put a voltage of –500 V on the repeller electrode and –380 V on the extractor electrode to collect the photoelectrons. Through tuning the axis of the motorized stage, we obtained a series of images of the electron momentum spectra with the same interval of the relative phase between the two colors. We recorded the photoelectron images for the relative phases changing over a range from 0 to 4π.

By using an iterative inversion procedure [31], the three-dimensional velocity distributions and the photoelectron angular distributions were retrieved. The ratio of the laser intensity between the second harmonic and the fundamental field is estimated from the frequency spectrum and the whole intensity of the laser pulse is calibrated by the shift of the ATI peak [30]. In the experiment, the intensity for the 400-nm laser field is $\sim 5.76 \times 10^{13}\,\mathrm{W/cm^2}$ and for the 800-nm laser field it is $\sim 4 \times 10^{13}\,\mathrm{W/cm^2}$. The absolute value of the relative phase between the two-color components is calibrated by comparisons with the numerical result.

B. Theoretical method

We use a semiclassical model to model the ionization of atoms in the two-color laser fields [32]. Firstly, we sample the electrons at the tunnel exit using the Monte Carlo method, in which the position of the tunnel exit is approximated given by $z_{\mathrm{exit}} = -I_p/E(t)$, where $E(t)$ is the instantaneous electric field of the laser pulse. The instantaneous tunneling ionization rate and the initial momentum distribution at the tunnel exit are given by the Ammosov-Delone-Krainov theory [33]. After tunneling the electron evolution in the combined oscillating laser field and Coulomb field is solved via the classical Newtonian equation $\ddot{\mathbf{r}} = -Z\mathbf{r}/r^3 - \mathbf{E}(t)$, where r is the distance between the electron and the nucleus and Z is the nuclear charge. Here the Coulomb potential and the external laser field are nonperturbatively included. At the end of the laser field, we select the electrons with positive energy and calculate the asymptotic momenta according to the Kepler's laws. The final photoelectron momentum spectrum is the sum of the ionization probability of all the trajectories in the momentum space. The parallel two-color laser field is given by $\mathbf{E}(t) = E_0 f(t)\cos(\omega t)\mathbf{z} + a E_0 f(t)\cos[2(\omega t + \varphi)]\mathbf{z}$, where $f(t)$ is the pulse envelope; E_0 and ω are the amplitude and frequency of the 800-nm fundamental laser field, respectively; a is the ratio of field strength of the two-color components; $\mathbf{z}$ is the unit vector in the laser polarization direction; φ is the relative phase of the two-color components. In the simulation, the laser envelope is a cosine square shape with 20 cycles of the 800-nm field in total.

III. RESULTS AND DISCUSSIONS

Figures 1(a)–1(c) show the measured two-dimensional photoelectron momentum distributions of Xe atoms in a two-color laser field with parallel polarizations at the relative phases of (a) $\varphi = 0$, (b) $\varphi = \pi/2$, and (c) $\varphi = \pi$, respectively. The photoelectron momentum distributions exhibit features which are similar to those in previous experiments using two-color laser fields [24,28]. First, all photoelectron momentum spectra show ringlike structures centered at zero momentum, which correspond to the ATI peaks in the energy spectrum. Second, each ATI peak exhibits an asymmetry along the laser polarization direction. At $\varphi = 0$, one can see that the electrons with positive final momenta (emitted in the forward direction) are greater in number than the electrons with negative final momenta (emitted in the backward direction), while at $\varphi = \pi$ the electrons emitted in the backward direction dominate over the electrons emitted in the forward direction. Moreover, one can find the asymmetric electron emission depends on the electron emission angle θ, where θ is the angle relative to the laser polarization direction.

In Figs. 2(a) and 2(b), we show the photoelectron angular distributions with respect to the relative phase for the first and second-order ATI, respectively. The modulations of the photoelectron yield with respect to the relative phase are different for the first-order and second-order ATI peaks. Due to the effect of the Coulomb potential, the modulation depth for the electrons emitted along the laser polarization direction is larger than that of electrons emitted transverse to the laser polarization direction for both the first-order and second-order

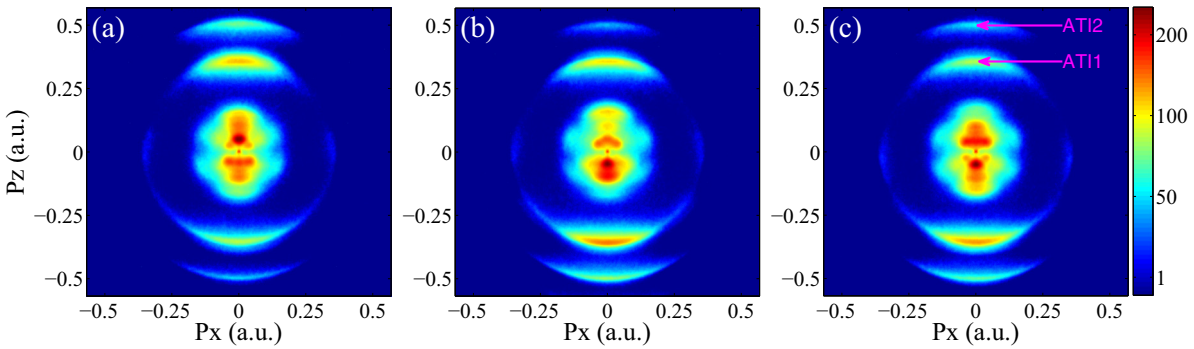

FIG. 1. The measured two-dimensional photoelectron momentum distributions of xenon atom in a two-color laser field at relative phases of (a) $\varphi = 0$, (b) $\varphi = \pi/2$, and (c) $\varphi = \pi$. The intensity for the 400-nm laser field is $\sim 5.76 \times 10^{13}$ W/cm^2 and for the 800-nm laser field it is $\sim 4 \times 10^{13}$ W/cm^2. The laser polarization direction is along the vertical direction.

ATI. Furthermore, there is a clear phase shift of $\sim 0.25\pi$ between the first-order and second-order ATI. This phase shift originates from the Coulomb correction of the parent ion to the interfering electron trajectories for the low-order ATI [24,28]. More interestingly, the yield of the electrons emitted along the laser polarization direction (near 0° and 180°) and transverse to the laser polarization direction (near 90°) shows different modulations with respect to the relative phase for the same-order ATI. Figures 2(c) and 2(e) show the ionization probability with the relative phase for the first-order ATI at $\theta = 0°$ and $\theta = 90°$, respectively. Figures 2(d) and 2(f) show the ionization probability with the relative phase for the second-order ATI at $\theta = 0°$ and $\theta = 90°$, respectively. For the first-order ATI, the yield has a maximum at $\sim 1.8\pi$ at the emission angle of 0° while the maximum shifts to $\sim 0.2\pi$ at the emission angle of 90°, as seen in Figs. 2(c) and 2(e). For the second-order ATI, the maximum of the yield locates at $\sim 1.55\pi$ at the emission angle of 0°, while it shifts to $\sim 1.65\pi$ at the emission angle of $\sim$90°, as seen in Figs. 2(d) and 2(f).

To show the angle-dependent electron emission in a quantitative way, we define the angle-dependent asymmetry parameter as $A(\theta,\varphi) = \frac{P(\theta,\varphi)-P(180-\theta,\varphi)}{P(\theta,\varphi)+P(180-\theta,\varphi)}$, where $P(\theta,\varphi)$ is the yield of the electron emitted along the angle θ at the relative phase φ. Next, we take the first-order ATI as an example. In Figs. 3(a), 3(d), and 3(g) we show the measured asymmetric parameter with respect to the relative phase at the emission angles of 0°, 50°, and 85° for the first-order ATI, respectively. One can see clear oscillations of the asymmetry parameter with respect to the relative phase. Those oscillations depend sensitively on the electron emission angle. For $\theta = 0°$, the maximum value of the asymmetry parameter locates at the relative phase of $\sim 1.75\pi$. For $\theta = 50°$, the maximum value slightly shifts to $\sim 1.45\pi$. For $\theta = 85°$, the maximum value locates at the relative phase of $\sim 0.3\pi$. There is a clear phase shift for the oscillations of the asymmetry parameters with respect to the relative phase as the emission angle increases. One can further see that the sign of the asymmetry parameter at 85° is opposite to that of 0° and 50° at some relative phases. For example, at $\varphi = 0.4\pi$ the asymmetry parameter is positive for $\theta = 85°$ while it is negative for $\theta = 0°$ and $\theta = 50°$.

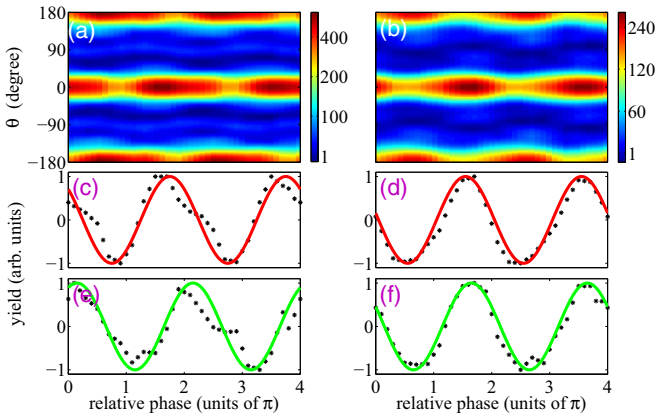

FIG. 2. The measured photoelectron angular distributions with respect to the relative phase for the (a) first- and (b) second-order ATI. (c,e) are the ionization probability of the first ATI with respect to the relative phase at $\theta = 0°$ and $\theta = 90°$, respectively. (d,f) are the ionization probability of the second-order ATI with respect to the relative phase at $\theta = 0°$ and $\theta = 90°$, respectively.

We use the semiclassical model to explain the physical origin of this angular-dependent asymmetry. We show the calculated asymmetry parameter with respect to the relative phase at the emission angle of 0° in Fig. 3(b), 50° in Fig. 3(e), and 85° in Fig. 3(h) for the first-order ATI without including the Coulomb potential and rescattering effect ($Z = 0$ in the Newtonian equation). One can find that the oscillation of the asymmetry parameter with respect to the relative phase is independent of the electron emission angle. The asymmetry curve with respect to the relative phase peaks at $\varphi = 0.5\pi$ for all emission angles because the vector potential of the laser field is the most asymmetric at this relative phase. We further show the calculated asymmetry parameter with respect to the relative phase at the emission angle of 0° in Fig. 3(c), 50° in Fig. 3(f), and 85° in Fig. 3(i), including the Coulomb potential and rescattering effect ($Z = 1$ in the Newtonian equation). Compared with the Coulomb-free case, the phase of the oscillation shifts due to the effect of the Coulomb tail [34,35]. One can further see that the oscillation of the asymmetry with respect to the relative phase differs for different emission angles. The asymmetry curve peaks at the relative phase of $\sim 1.75\pi$ for $\theta = 0°$, $\sim 1.6\pi$ for $\theta = 50°$, and $\sim 0.4\pi$ for $\theta = 85°$, which qualitatively agree with the measurement. The qualitative agreement

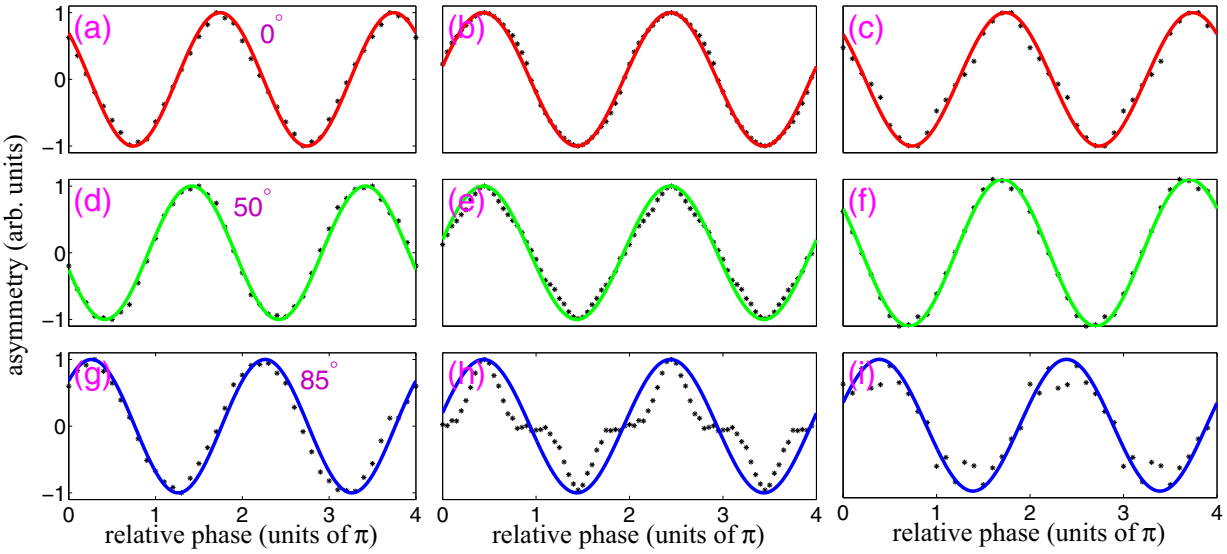

FIG. 3. The asymmetry curves with respect to the relative phase at the electron emission angles of 0°, 50°, and 85° from the experimental data (a),(d),(g), the semiclassical simulation without the Coulomb potential (b),(e),(h), and the semiclassical simulation including the Coulomb potential (c),(f),(i) for the first-order ATI. The solid lines are used to guide the modulation of the asymmetry parameters.

between the measurement and the simulation indicates that the Coulomb potential and rescattering effect is responsible for the angular-dependent asymmetries in the two-color laser fields.

To show how the Coulomb potential and rescattering effect influences the dependence of the asymmetry on the relative phase, we need to separate the contributions of different trajectories to the photoelectron angular distributions. As known, both nonscattering electrons and rescattering electrons contribute to the formation of the photoelectron angular distribution of the ATI [4]. The nonscattering trajectories mainly contributed to the low-energy photoelectrons. Those nonscattering trajectories experience Coulomb focusing effects and their final transverse momenta are slightly smaller than the initial momentum at the tunnel exit. Thus the signs of the final transverse momenta of the nonscattering electrons are the same as that of the initial transverse momenta. For the rescattering trajectories, the rescattering process leads to sign reversal of their transverse momenta [36]. Thus we can separate the relative contributions of those two kinds of trajectories within the semiclassical model.

We show the ionization probabilities of the nonscattering ($p_x v_x > 0$), and rescattering ($p_x v_x < 0$) trajectories with respect to the electron emission angle and the relative phase for the first-order ATI in Figs. 4(a) and 4(b), respectively. Here p_x is the final transverse momenta relative to the laser polarization direction, and v_x is the initial transverse momentum at the tunnel exit. One can see that the relative contributions of the rescattering trajectories and nonscattering trajectories reveal different oscillations with respect to the relative phase. For the emission angle of 0°, the ionization probability of the nonscattering trajectory has a maximum at the relative phase of $\sim 1.5\pi$. At this relative phase, the vector potential of the laser field is the most asymmetric, leading to the electrons being mostly emitted at ∼0°. Because the rescattering electrons are mainly released after the field maximum, the maximum of the ionization probability of the rescattering trajectory shifts to the relative phase of $\sim 1.8\pi$, as seen in Fig. 4(b). More importantly, some of the rescattering trajectories can be emitted to a large angle with respect to the laser polarization direction, which depends sensitively on the relative phase. For example, for the emission angle between 60° and 120°, the relative contribution of the rescattering trajectory is larger or smaller than that of the nonscattering trajectory depending on the relative phase. For the electrons emitted along the laser polarization direction, the relative contribution of the nonscattering trajectory is usually dominant over that of the rescattering trajectory. Thus the yield of the electrons emitted to different angles shows different modulations with respect to the relative phase. The relative contributions of the rescattering and nonscattering trajectories differ considerably at different emission angles, thus leading to the angular-dependent asymmetry in Fig. 3.

The following two reasons might be responsible for the small difference of the maximum position between the simulation and the measurement in Fig. 3. Firstly, the spatial and temporal overlap of the 800- and 400-nm pulses in the

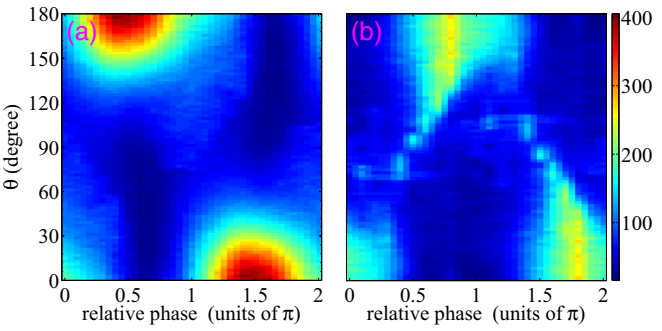

FIG. 4. The calculated ionization probabilities with respect to the electron emission angle and the relative phase for the nonscattering electrons (a) and rescattering electrons (b) for the first-order ATI. Note that the color scale is the same for both plots.

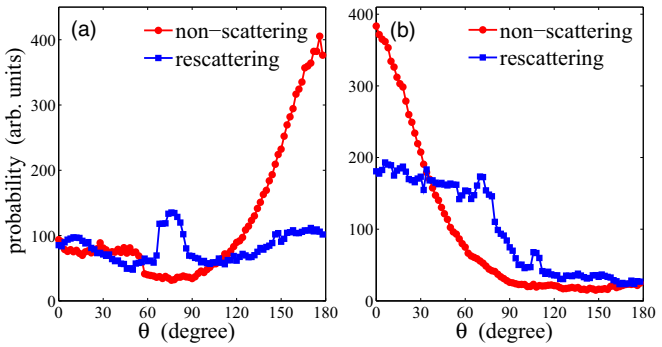

FIG. 5. The calculated ionization probability of the nonscattering and rescattering trajectories with respect to the electron emission angle at the relative phases of 0.4π (a) and 1.6π (b) for the first-order ATI.

experiment is not as perfect as assumed in the calculation. Secondly, the semiclassical model based on ADK tunneling theory and the classical Newtonian equation might not be very accurate to describe the relative contributions of the nonscattering and rescattering trajectories in different emission angles. The relative contributions of rescattering trajectories might be underestimated by the simulation at the emission angles of 50° and 85°.

In Fig. 5, we show the ionization probability of the nonscattering and rescattering trajectories with respect to the emission angle at the relative phase of 0.4π and 1.6π. The relative phases of 0.4π and 1.6π correspond to the maximum of the asymmetry parameter for the emission angles of 85° and 50°, respectively. At the relative phase of 0.4π [Fig. 5(a)], there is an enhancement of the electron yield at the emission angle from 60° to 90° for the rescattering electrons, showing a hump structure at the emission angle of 60°–90°. Thus the electrons emitted nearly perpendicular to the polarization direction are dominated by the contributions of the rescattering trajectories, while at the emission angle of 180° the electrons are dominated by the contributions of the nonscattering electrons. For the electrons emitted nearly along the laser polarization direction, there are more electrons emitted along ∼180° than the electrons emitted along ∼0°. Thus the asymmetry parameter at $\theta = 0°$ is negative. For the electrons emitted almost perpendicular to the laser polarization direction, there are fewer electrons emitted along ∼95° than along ∼85° because of the enhancement of the yield of the rescattering trajectories at the emission angle of 60°–90°. Therefore the asymmetry parameter at the emission angle of 85° is positive.

At the relative phase of 1.6π [Fig. 5(b)], the nonscattering trajectories are mainly emitted along the laser polarization direction (smaller than 30°). The yield of the rescattering trajectories with respect to the emission angle shows a distribution ranging from 0° to 60°, whose width is larger than that of the nonscattering trajectories. Thus the electrons along near ∼0° are dominated by the nonscattering trajectory and the electrons along ∼50° are dominated by the rescattering trajectory. Because the nonscattering and rescattering trajectories are mainly emitted to the forward direction, the asymmetry parameters are positive for both $\theta = 0°$ and $\theta = 50°$. Moreover, the oscillations of the yield with respect to the relative phase for the nonscattering electrons and rescattering electrons reveal a small phase shift, as seen in Figs. 4(a) and 4(b); thus the asymmetry parameter with respect to the relative phase also reveals a slight phase shift for those two emission angles.

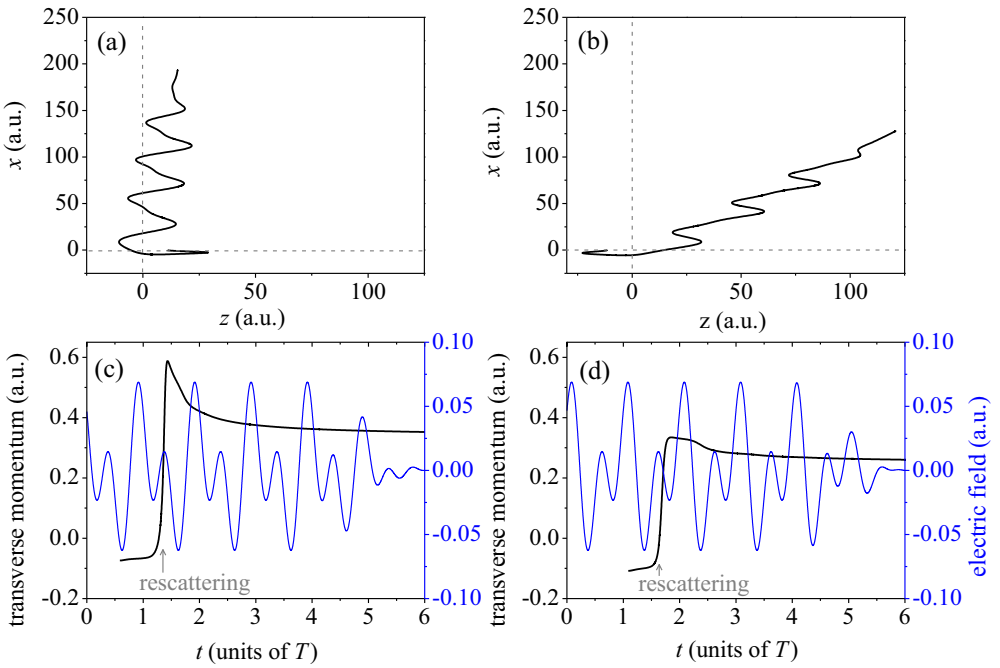

FIG. 6. (a),(b) show the typical rescattering trajectories at the relative phases of 0.4π (emitted at ∼85°) and 1.6π (emitted at ∼50°), respectively. (c),(d) show the time revolution of the transverse momentum of the electron trajectories in (a),(b), respectively. The corresponding electric fields are shown with the blue lines in (c),(d). The arrows in (c),(d) show the instant of the rescattering.

To shed more light on the dependence of the electron emission angle on the relative phase for the rescattering trajectory, we now trace the trajectories of the rescattering electrons. In Figs. 6(a) and 6(b), we show the typical rescattering trajectories at the relative phase of 0.4π and 1.6π, respectively. Figures 6(c) and 6(d) show the time evolution of the electron transverse momenta, corresponding to the trajectories in Figs. 6(a) and 6(b), respectively. At the relative phase of 0.4π [Figs. 6(a) and 6(c)], the rescattering electron is driven back by the laser field at nearly $0.8T$ after tunneling (T is the cycle of the 800-nm laser field) with a small initial transverse momentum of $\sim$0.08 a.u. at the tunnel exit. Thus the electron has a small lateral distance of $\sim$4.3 a.u. from the parent ion when the laser field drives it back along the longitudinal direction relative to the laser polarization. The electron is directly pulled by the strong Coulomb potential to the nucleus and scattered forward with a large angle at the instant of the scattering. Thus the electron has a large possibility to be emitted transverse to the laser polarization direction. At the relative phase of 1.6π [Figs. 6(b) and 6(d)], the rescattering electron is driven back at $\sim 0.5T$ after tunneling. Compared with Fig. 6(a), the electron has a larger initial transverse momentum of $\sim$0.11 a.u. at the tunnel exit and a larger lateral distance of $\sim$6.1 a.u. from the parent ion at the instant of the scattering. Therefore, the electron is influenced by a smaller Coulomb effect, leading to a smaller scattering angle at the instant of the scattering. Accordingly, at the relative phase of 1.6π, it is easy for the rescattering electron to be scattered to the directions with a small angle relative to the laser polarization [Fig. 5(b)].

As shown above, the emission angle of the rescattering trajectory depends on the difference between the rescattering time and the birth time as well as the initial transverse momentum at the tunnel exit. By tuning the relative phase of the parallel two-color laser field, we can control the electron emission angle of the rescattering trajectory. It has been demonstrated before that the rescattering electrons in space and time can be controlled using orthogonally polarized two-color laser pulses, where the laser field in two spatial dimensions with different frequencies gives full control over the electron wave packets [14,21]. Here we show that although the laser field is in one spatial dimension, we can also control the electron emission angle of the rescattering electron by controlling the subcycle laser shape, as seen in Fig. 4(b). Since the relative phase of 0.1π corresponds to $T/20 = 133$ as, the emission angle can be controlled with attosecond precision, according to the semiclassical model.

IV. CONCLUSION

In summary, we have measured the photoelectron momentum spectra from above-threshold ionization of Xe atoms in a linearly polarized two-color laser field at a serial of relative phases. Depending on the electron emission angle and the relative phase, the electron yield show obvious forward-backward asymmetries along the laser polarization direction. With increasing the emission angle relative to the polarization direction, a phase shift in the asymmetry curve as a function of the two-color relative phase is observed. Based on a semiclassical model, we separate the relative contributions of the nonscattering and the rescattering trajectories on the photoelectron angular distributions of the above-threshold ionization and show that the rescattering electrons make a non-negligible contribution to the formation of the photoelectron angular distributions in the two-color laser field. Depending on the relative phase between the two colors, the rescattering trajectories can be emitted to the direction with a large angle relative to the laser polarization, and the electrons along the laser polarization direction are mainly dominated by the nonscattering trajectories. The relative contributions of the nonscattering and the rescattering trajectories differ significantly for different emission angles, leading to the angular-dependent asymmetry. By tuning the relative phase of the two-color pulse, the electron emission angle and the relative contributions of the rescattering trajectories can be precisely controlled.

ACKNOWLEDGMENTS

This work was supported by the National Natural Science Foundation of China under Grants No. 61405064, No. 11674116, No. 11234004, and No. 11422435 and the Fundamental Research Funds for the Central University (HUST: 2016YXMS012).

[1] P. Agostini, F. Fabre, G. Mainfray, G. Petite, and N. K. Rahman, Phys. Rev. Lett. **42**, 1127 (1979).

[2] L. V. Keldysh, Zh. Eksp. Teor. Fiz. **47**, 1945 (1964) [Sov. Phys. JETP **20**, 1307 (1965)].

[3] Ph. A. Korneev, S. V. Popruzhenko, S. P. Goreslavski, T.-M. Yan, D. Bauer, W. Becker, M. Kübel, M. F. Kling, C. Rödel, M. Wünsche, and G. G. Paulus, Phys. Rev. Lett. **108**, 223601 (2012).

[4] M. Li, J.-W. Geng, H. Liu, Y. Deng, C. Wu, L.-Y. Peng, Q. Gong, and Y. Liu, Phys. Rev. Lett. **112**, 113002 (2014).

[5] G. G. Paulus, W. Nicklich, H. Xu, P. Lambropoulos, and H. Walther, Phys. Rev. Lett. **72**, 2851 (1994).

[6] Y. Huismans, A. Rouzée, A. Gijsbertsen, J. H. Jungmann, A. S. Smolkowska, P. S. W. M. Logman, F. Lépine, C. Cauchy, S. Zamith, T. Marchenko, J. M. Bakker, G. Berden, B. Redlich, A. F. G. van der Meer, H. G. Muller, W. Vermin, K. J. Schafer, M. Spanner, M. Yu. Ivanov, O. Smirnova *et al.*, Science **331**, 61 (2011).

[7] Y. Zhou, O. I. Tolstikhin, and T. Morishita, Phys. Rev. Lett. **116**, 173001 (2016).

[8] J. Itatani, J. Levesque, D. Zeidler, H. Niikura, H. Pépin, J. C. Kieffer, P. B. Corkum, and D. M. Villeneuve, Nature (London) **432**, 867 (2004); P. Lan, M. Ruhmann, L. He, C. Zhai, F. Wang, X. Zhu, Q. Zhang, Y. Zhou, M. Li, M. Lein, and P. Lu, Phys. Rev. Lett. **119**, 033201 (2017).

[9] M. Meckel, D. Comtois, D. Zeidler, A. Staudte, D. Pavičić, H. C. Bandulet, H. Pépin, J. C. Keiffer, R. Dörner, D. M. Villeneuve, and P. B. Corkum, Science **320**, 1478 (2008).

[10] H. Akagi, T. Otobe, A. Staudte, A. Shiner, F. Turner, R. Dörner, D. M. Villeneuve, and P. B. Corkum, Science **325**, 1364 (2009).

[11] D. N. Fittinghoff, P. R. Bolton, B. Chang, and K. C. Kulander, Phys. Rev. Lett. **69**, 2642 (1992); B. Walker, B. Sheehy, L. F. DiMauro, P. Agostini, K. J. Schafer, and K. C. Kulander, *ibid.* **73**, 1227 (1994).

[12] A. McPherson, G. Gibson, H. Jara, U. Johann, T. S. Luk, I. A. McIntyre, K. Boyer, and C. K. Rhodes, J. Opt. Soc. Am. B **4**, 595 (1987).

[13] M. Ferray, A. L'Huillier, X. F. Li, L. A. Lompre, G. Mainfray, and C. Manus, J. Phys. B **21**, L31 (1988).

[14] M. Kitzler and M. Lezius, Phys. Rev. Lett. **95**, 253001 (2005).

[15] P. Agostini, P. Breger, A. L'Huillier, H. G. Muller, G. Petite, A. Antonetti, and A. Migus, Phys. Rev. Lett. **63**, 2208 (1989).

[16] D. W. Schumacher and P. H. Bucksbaum, Phys. Rev. A **54**, 4271 (1996).

[17] D. Ray, Z. Chen, S. De, W. Cao, I. V. Litvinyuk, A. T. Le, C. D. Lin, M. F. Kling, and C. L. Cocke, Phys. Rev. A **83**, 013410 (2011); L. Zhang, X. Xie, S. Roither, D. Kartashov, Y. L. Wang, C. L. Wang, M. Schöffler, D. Shafir, P. B. Corkum, A. Baltuška, I. Ivanov, A. Kheifets, X. J. Liu, A. Staudte, and M. Kitzler, *ibid.* **90**, 061401(R) (2014).

[18] D. G. Arbó, C. Lemell, S. Nagele, N. Camus, L. Fechner, A. Krupp, T. Pfeifer, S. D. López, R. Moshammer, and J. Burgdörfer, Phys. Rev. A **92**, 023402 (2015).

[19] M. Richter, M. Kunitski, M. Schöffler, T. Jahnke, L. P. H. Schmidt, M. Li, Y. Liu, and R. Dörner, Phys. Rev. Lett. **114**, 143001 (2015).

[20] J.-W. Geng, W.-H. Xiong, X.-R. Xiao, L.-Y. Peng, and Q. Gong, Phys. Rev. Lett. **115**, 193001 (2015); M. Li, J.-W. Geng, M.-M. Liu, X. Zheng, L.-Y. Peng, Q. Gong, and Y. Liu, Phys. Rev. A **92**, 013416 (2015).

[21] M. He, Y. Li, Y. Zhou, M. Li, and P. Lu, Phys. Rev. A **93**, 033406 (2016).

[22] L. Zhang, X. Xie, S. Roither, Y. Zhou, P. Lu, D. Kartashov, M. Schöffler, D. Shafir, P. B. Corkum, A. Baltuška, A. Staudte, and M. Kitzler, Phys. Rev. Lett. **112**, 193002 (2014); Y. Zhou, C. Huang, A. Tong, Q. Liao, and P. Lu, Opt. Express **19**, 2301 (2011).

[23] X. Gong, P. He, Q. Song, Q. Ji, H. Pan, J. Ding, F. He, H. Zeng, and J. Wu, Phys. Rev. Lett. **113**, 203001 (2014).

[24] L. Zipp, A. Natan, and P. H. Bucksbaum, Optica **1**, 361 (2014).

[25] X. Xie, S. Roither, D. Kartashov, E. Persson, D. G. Arbó, L. Zhang, S. Gräfe, M. S. Schöffler, J. Burgdörfer, A. Baltuška, and M. Kitzler, Phys. Rev. Lett. **108**, 193004 (2012); D. G. Arbó, S. Nagele, X.-M. Tong, X. Xie, M. Kitzler, and J. Burgdörfer, Phys. Rev. A **89**, 043414 (2014).

[26] D. Shafir, H. Soifer, B. D. Bruner, M. Dagan, Y. Mairesse, S. Patchkovskii, M. Yu. Ivanov, O. Smirnova, and N. Dudovich, Nature **485**, 343 (2012).

[27] J. Zhao and M. Lein, Phys. Rev. Lett. **111**, 043901 (2013).

[28] X. Gong, C. Lin, F. He, Q. Song, K. Lin, Q. Ji, W. Zhang, J. Ma, P. Lu, Y. Liu, H. Zeng, W. Yang, and J. Wu, Phys. Rev. Lett. **118**, 143203 (2017).

[29] S. Skruszewicz, J. Tiggesbäumker, K.-H. Meiwes-Broer, M. Arbeiter, Th. Fennel, and D. Bauer, Phys. Rev. Lett. **115**, 043001 (2015).

[30] M. Li, P. Zhang, S. Luo, Y. Zhou, Q. Zhang, P. Lan, and P. Lu, Phys. Rev. A **92**, 063404 (2015).

[31] M. J. J. Vrakking, Rev. Sci. Instrum. **72**, 4084 (2001).

[32] B. Hu, J. Liu, and S. G. Chen, Phys. Lett. A **236**, 533 (1997).

[33] M. V. Ammosov, N. B. Delone, and V. P. Krainov, Sov. Phys. JETP **64**, 1191 (1986); N. B. Delone and V. P. Krainov, J. Opt. Soc. Am. B **8**, 1207 (1991).

[34] A. D. Bandrauk and S. Chelkowski, Phys. Rev. Lett. **84**, 3562 (2000).

[35] S. Chelkowski, M. Zamojski, and A. D. Bandrauk, Phys. Rev. A **63**, 023409 (2001).

[36] H. Xie, M. Li, Y. Li, Y. Zhou, and P. Lu, Opt. Express **24**, 27726 (2016).